Zr^{4+}) ions gives rise to essentially equal (Mg,Zr)–O bond distances of 2·12 (1) Å. This constraint of constant bond distance coupled with the net electrostatic repulsion between (Mg^{2+},Zr^{4+}) ions in the **c** direction causes the oxygens to be displaced from their ideal value of 0·125 (Table 1). Consequently, the less-polarizing Li^+ ions are forced to accept two abnormally long Li–O bonds of 2·44 (2) Å in the **c** direction. As further evidence of the repulsion between edge-sharing (Mg,Zr)O_6 octahedra, the oxide ions that form these common edges are separated by only 2·888 Å, giving a reduced O–(Mg,Zr)–O angle of 85·8 (3)°. For undistorted (Mg,Zr)O_6 octahedra with angles of 90° and the same (Mg,Zr)O_6 bond length, the oxygen–oxygen edges would be 3·107 Å. This closer approach of the oxide ions in the edge-sharing (Mg,Zr)O_6 octahedra serves both to push apart the (Mg^{2+}/Zr^{4+}) cations on either side and partially to shield their positive charges from each other.

The isotropic temperature factor for lithium (Table 1) is anomalously low. This may be an artefact associated with the limited data set that was available; also the e.s.d. is relatively large.

Various oxides $LiMO_2$, M = trivalent ion, form the α-$LiFeO_2$ structure but Li_2MgZrO_4 is the first to contain three cations. This is made possible by the similar size/coordination requirements of Mg^{2+} and Zr^{4+}, which typically have octahedral bond distances to oxygen of ~2·12 Å (Shannon & Prewitt, 1969, 1970) and which allows them to be disordered over the Fe^{3+} sites, without incurring additional major structural distortions.

MC thanks CONACYT for a research grant, No. PCCBBNA001886.

ARW thanks the British Council for financial assistance in support of the Aberdeen–Mexico collaboration programme. We thank R. A. Howie for help with the computing, which was carried out at the University of Aberdeen Computer Centre.

References

AHMED, F. R., HALL, S. R., PIPPY, M. E. & HUBER, C. P. (1973). *NRC Crystallographic Programs for the IBM/360 System.* National Research Council, Ottawa, Canada. Modified for use on the Honeywell 66/80 machine of the Computing Centre, Univ. of Aberdeen, by S. J. KNOWLES, H. F. W. TAYLOR & R. A. HOWIE.

International Tables for X-ray Crystallography (1962). Vol. III. Birmingham: Kynoch Press. (Present distributor D. Reidel, Dordrecht.)

POSNJAK, E. & BARTH, T. F. W. (1931). *Phys. Rev.* **38**, 2234–2239.

SHANNON, R. D. & PREWITT, C. T. (1969). *Acta Cryst.* B**25**, 925–946.

SHANNON, R. D. & PREWITT, C. T. (1970). *Acta Cryst.* B**26**, 1046–1048.

WYCKOFF, R. G. (1964). *Crystal Structures,* Vol. 2, pp. 312–314. New York: Interscience.

Acta Cryst. (1985). C**41**, 1709–1714

The Structures of Trithallium Tetraselenophosphate and Trithallium Tetrathioarsenate at 65 K

BY R. W. ALKIRE, ALLEN C. LARSON AND PHILLIP J. VERGAMINI

Los Alamos National Laboratory, Los Alamos, New Mexico 87545, *USA*

AND BRUNO MOROSIN

Sandia National Laboratories, Albuquerque, New Mexico 87185, *USA*

(*Received* 2 *April* 1985; *accepted* 14 *June* 1985)

Abstract. Low-temperature (65 K) single-crystal neutron structure determinations were performed on the isostructural materials Tl_3PSe_4 and Tl_3AsS_4 using a newly designed single-crystal diffractometer at the Los Alamos National Laboratory Pulsed Neutron Facility. For Tl_3PSe_4: $M_r = 959·92$, *Pcmn*, $a = 9·291$ (2), $b = 10·991$ (3), $c = 9·041$ (2) Å, $V = 923·30$ Å^3, $Z = 4$, $D_x = 6·905$ Mg m^{-3}, $\lambda_{neutron} = 0·75 \rightarrow 4·2$ Å, $F(000) = 252·5$ fm. For Tl_3AsS_4: $M_r = 816·29$, *Pcmn*, $a = 9·089$ (2), $b = 10·803$ (2), $c = 8·867$ (2) Å, $V = 870·60$ Å^3, $Z = 4$, $D_x = 6·227$ Mg m^{-3}, $\lambda_{neutron} = 0·75 \rightarrow 4·2$ Å, $F(000) = 177·2$ fm. For Tl_3PSe_4 (Tl_3AsS_4) 2335 (2678) reflections were measured with $I > 3\sigma(I)$ and refined by full-matrix least squares to $R(F) = 0·049$ (0·053). Results of atomic-parameter refinement from this study yield an increase in precision by a factor of two over a previous single-crystal neutron structural study at room temperature (293 K). Deviation of the PSe_4^{3-} (AsS_4^{3-}) group from an idealized tetrahedral arrangement is significant and one Tl^+ ion

0108-2701/85/121709-06$01.50

shows large anisotropic thermal motion, which is consistent with the room-temperature structure. Employing distances corrected for thermal motion, one is able to reconcile the anisotropic thermal expansion behavior of these materials. Previous measurements of the ultrasonic velocity in these materials as a function of pressure and temperature suggested that temperature-induced phase transitions would not be observed at low temperature. The present results, together with recent high-pressure data on Tl_3PSe_4, support this prediction.

Introduction. Tl_3PSe_4 and Tl_3AsS_4 are members of a growing family of chalcogenide crystals with possible applications in acousto-optic devices. Synthesis and characterization of the title compounds by Gottlieb, Isaacs, Feichtner & Roland (1974) have shown that the optical transmission for these materials is good, 60–90% in the 0·8→8 μm region, and their acoustic (shear-wave) velocities are among the lowest of any solid or liquid recorded in the literature. Figures of merit measured for Tl_3PSe_4 and Tl_3AsS_4 are quite high, with comparatively few materials performing as well for wavelengths in the near infrared region.

Measured ultrasonic velocities for wave propagation along the principal crystallographic axes at ambient temperature and pressure have revealed anomalously low *ab* shear mode velocities for both compounds. High-pressure ultrasonic (pulse echo) data on Tl_3PSe_4 show the anomalous shear velocity softens to zero at 1·40 GPa, indicating a second-order structural phase transition at that pressure (Fritz, Isaacs, Gottlieb & Morosin, 1978, hereafter FIGM, 1978). Identical measurements on Tl_3AsS_4 (Fritz, Gottlieb, Isaacs & Morosin, 1981) showed two structural phase transitions at 2·1 and 2·6 GPa; the first transition occurs before the soft mode reaches zero velocity. In an attempt to determine whether the Tl_3PSe_4 transition could be driven by temperature, ultrasonic measurements were performed down to 90 K and the results showed a 25% softening of the shear velocity, spread out uniformly over the entire temperature range (FIGM, 1978). However, owing to failure of the transducer bonds, lower temperatures were unattainable and, without definitive structural evidence, these authors were uncertain as to whether the transition could be driven by temperature alone.

X-rays were originally used to determine atomic positions for these materials (FIGM, 1978) but standard deviations were high owing to difficulties in correcting for absorption. Recently, a neutron diffraction study was conducted by the authors at 293 K using time-of-flight (TOF) techniques (Alkire, Vergamini, Larson & Morosin, 1984). Room-temperature measurements showed an unusually large anisotropic thermal parameter for the Tl(2) ion in both compounds (related to atomic arrangement) and deviations from tetrahedral geometry in the PSe_4^{3-} (AsS_4^{3-}) group. The purpose of the current work is to ascertain whether a phase transition occurs (or can occur) in these materials at low temperature and to determine atomic parameters, with particular interest centered on changes occurring in the Tl(2) ion.

Experimental. The newly constructed single-crystal neutron diffractometer at Los Alamos National Laboratory has been designed with an unusually large open environment around the sample position to accommodate a wide variety of special environmental devices (Vergamini, Larson & Alkire, 1985). This has been accomplished by replacing the standard χ motion with a fixed χ bracket ($\chi = 60°$, see Fig. 1). A closed-cycle refrigerator, designed as an integral part of the φ motion, is mounted on the χ bracket. In order to accommodate helium transfer lines, both φ and ω have been limited to approximately 350° of travel. The detector, a Borkowski–Kopp-type position-sensitive proportional counter (Borkowski & Kopp, 1978), is filled with 3×10^5 Pa (total) of $^3He + Xe + CO_2$, has an active area of 25 × 25 cm and is mounted on rails inside a B_4C-lined container; detector position is fixed at a nominal 90° 2θ. To maximize reciprocal-space coverage with this geometry, the detector is elevated (by means of an arc drive) above the crystal position. Angular (vertical) range, referenced to detector center, is from 30° (minimum) to 50° (maximum). Because the detector is free to move inside the shielding container, sample-to-detector distance can be varied from 26 to 50 cm.

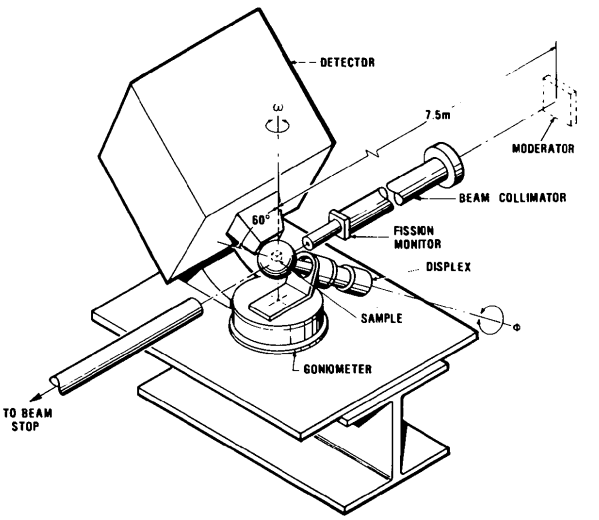

Fig. 1. Los Alamos National Laboratory single-crystal neutron diffractometer designed for time-of-flight operation, using a 25 × 25 cm position-sensitive detector and a fixed χ geometry. Without the geometric constraints imposed by a standard full circle, the open sample environment allows maximum flexibility for installing special environmental devices.

When conducting experiments using TOF diffraction techniques in combination with a position-sensitive area detector, it is important to realize that special environment windows, *e.g.* an aluminium vacuum shroud, are generally polycrystalline. As incident (white-beam) radiation passes through the shroud, diffraction from the aluminium occurs at virtually all wavelengths. Geometric factors imposed by detector width, sample-to-detector distance and vacuum-shroud diameter prevent complete shielding against this unwanted radiation. One solution is to change from spherical to cylindrical geometry, moving the incident-beam entrance and exit windows of the vacuum shroud far from the detector opening, and then adding rotating vacuum seals to accommodate crystal motion; this technique is currently in use at Argonne National Laboratory (Schultz, 1984). However, with our fixed-χ geometry, rotating vacuum seals would be difficult to install and, more importantly, might restrict our open sample environment. Instead, we have chosen to install a single vertically oriented Cd Soller slit in the center of the detector. At a cost of 10% of the detecting area, this effectively shields against background radiation produced by the vacuum shroud.

For this study, sample-to-detector distance was 26 cm and sample-to-moderator distance was 752 cm. Each event on the detector was encoded within a framework consisting of 64 × 64 spatial (x,y) channels and a time resolution of 188 channels, covering a wavelength range of 0·75→4·2 Å. Time channels were divided into nearly equal increments of $1/d$ and individual x,y channels were equally spaced across the detector.*

The single crystals of Tl_3PSe_4 (Tl_3AsS_4) used in the room-temperature neutron diffraction study, dimensions 2·96 × 2·86 × 2·86 mm (2·90 × 2·80 × 2·60 mm), were used for the present work. Low-temperature measurements were made without surrounding the samples with an internal radiation shield. Sample temperature calibrations made after data collection using a copper–constantan differential thermocouple revealed sample temperatures to be 65 (3) K.† Initial lattice parameters were taken from the previous room-temperature (293 K) neutron diffraction study [Tl_3PSe_4: $a = 9{\cdot}276$ (1), $b = 11{\cdot}036$ (2), $c = 9{\cdot}058$ (1) Å; Tl_3AsS_4: $a = 9{\cdot}084$ (3), $b = 10{\cdot}877$ (3), $c = 8{\cdot}877$ (3) Å] and further refined using peak positions from 627 (744) reflections measured in the range 66→114° 2θ. Space group *Pcmn* (*cba* setting of *Pnma*; general positions $\pm x, y, z$; $\pm\frac{1}{2}-x, y, \frac{1}{2}+z$; $\pm x, \frac{1}{2}-y, z$; $\pm\frac{1}{2}-x, \frac{1}{2}-y, \frac{1}{2}+z$) was retained for these structures to remain consistent with earlier X-ray and neutron work. Neutron transmission values were 0·93→0·87 (0·97→0·93); nuclear scattering lengths (fm) used in this study: Tl = 8·8, P = 5·1, Se = 8·0, As = 6·6, S = 2·8 (Koester & Yelon, 1982). Absence of neutron resonances in the 0·75→4·2 Å wavelength range for Tl, P, Se, As and S (Mughabghab & Garber, 1973; Garber & Kinsey, 1976) allows linear absorption coefficients to be calculated as follows: Tl_3PSe_4: $\mu(cm^{-1}) = 0{\cdot}286 + 0{\cdot}069\lambda$; Tl_3AsS_4: $\mu(cm^{-1}) = 0{\cdot}179 + 0{\cdot}021\lambda$.

Thirteen histograms were collected on Tl_3PSe_4 (approximately one independent unit of data with some overlap between adjacent histograms; measuring time per histogram 4 h) covering $h = -8,18$, $k = -6,21$, $l = \pm 17$ with 3579 reflections measured, 2355 observed (2095 unique) with $I > 3\sigma(I)$; sixteen histograms were measured on Tl_3AsS_4, $h = \pm 18$, $k = -4,21$, $l = -3,17$ with 4198 reflections measured, 2678 observed (2498 unique) with $I > 3\sigma(I)$; max. $\sin\theta/\lambda$ in least-squares refinement was 1·00 (1·00) Å^{-1}. Owing to the variation of extinction and absorption with wavelength in TOF diffraction, all measured reflections were treated as independent observations, *i.e.* 'equivalent' reflections were not averaged. Internal consistency index for reflections measured more than once after appropriate absorption and extinction correction was 3·6% for Tl_3PSe_4 and 4·4% for Tl_3AsS_4. Data reduction and least-squares refinement were performed using the Los Alamos crystal structure programs (Larson, 1977) and Fig. 2 was drawn using *ORTEP*II (Johnson, 1976).

Refinements of both structures were carried out using anisotropic temperature factors and an isotropic extinction parameter. Initial positional parameters were taken from the previous neutron diffraction study and

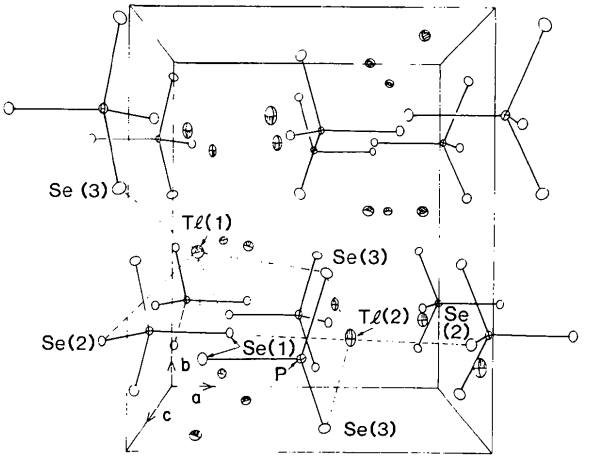

Fig. 2. Tl_3PSe_4 unit-cell packing (at 65 K, shown with 50% probability ellipsoids) as viewed along the c axis; dashed lines illustrate the Tl---Se environment within a radius of 3·4 Å.

* For a general description of the TOF technique see, for example, Alkire *et al.* (1984).

† Since the time of this study an internal radiation shield has been developed, specifically for use with an area detector, allowing sample temperature to reach 11 K without any measurable increase in background radiation.

final least-squares refinement cycles for Tl_3PSe_4 (Tl_3AsS_4) yielded $R(F) = 0.049$ (0.053), $wR(F) = 0.042$ (0.047), $S = 2.27$ (2.17) with $w = [1/\sigma(F_o)]^2$; $(\Delta/\sigma)_{max}$ in the final refinement cycle was 3.5×10^{-4} (1.9×10^{-4}); secondary-extinction modeling of type I yielded a Gaussian half-width of 0.8° (0.4°).

Discussion. Tl_3PSe_4 and Tl_3AsS_4 are isostructural materials, consisting of layers situated about mirror planes normal to the *b* axis at $y = \pm\frac{1}{4}$. For each Tl_3PSe_4 formula unit, one Tl, the P and two Se atoms lie on the mirror plane, and the remaining two Tl and two Se atoms are symmetrically disposed about the plane. At reduced temperature, both compounds exhibit a small but significant lattice expansion in the **a** direction along with contractions in the **b** and **c** directions, compared to room-temperature values. Contraction along the **b** direction, *i.e.* between layers, is significantly larger than contraction in the **c** direction, with Tl_3AsS_4 showing the largest effect; Fig. 2 illustrates the Tl_3PSe_4 structure as viewed along the *c* axis. Table 1 lists refined positional* and thermal parameters for Tl_3PSe_4 and Tl_3AsS_4, and Table 2 lists comparative bond distances and angles for both 65 and 293 K structures; these values have not been adjusted for thermal motion. Table 3 lists comparative distances for both structures that have been corrected for thermal motion; significant differences ($>3\sigma$) are present for a large number of separations based on standard deviations from the uncorrected distances.

Analysis of the structural changes occurring in these materials upon cooling depends largely on how one interprets the atomic thermal motion, particularly at room temperature. P—Se(X) and As—S(X) distances ($X = 1,2,3$) have been corrected for thermal motion using the Busing & Levy (1964) model for riding motion. These values should represent upper limits to the P—Se(X) and As—S(X) bond lengths, with actual distances intermediate between the corrected and uncorrected values. Tl(X) electrostatic interaction distances have been adjusted for thermal motion using the Busing & Levy (1964) model for non-correlated motion. Tl(X)---Se(X) and Tl(X)---S(X) distances corrected for non-correlated motion accurately reflect changes in Tl(X) atomic separations and these values are used when interpreting Tl(X) electrostatic interactions.

Using Tl_3PSe_4 to illustrate the effects of cooling, lattice contraction along the **b** direction reflects a decrease in the inter-layer separation, with a corresponding shortening of the inter-layer Tl(1)---Se(3) distance. Principal change along the **c** direction involves reduction of the Tl(2)---Se(3) interaction distance (ranging from 0.01 to 0.02 Å in both structures) and a slight reduction in distance between intra-layer tetrahedra.

The trend in both structures is for all tetrahedral bonds to become elongated at low temperature. In addition, all intra-layer Tl(1)---Se(X) electrostatic contacts either expand or remain essentially unchanged. One explanation that would account for the **a** lattice expansion involves a redistribution of charge in the P—Se(3)→Tl(2) region. As Tl(2) approaches the PSe_4^{3-} group, Tl(2)---Se(3) contacts are strengthened and, therefore, P—Se(X) bonds are weakened (elongated). As P—Se(X) bonds lengthen, relative tetrahedra separation is maintained by Tl(1)---Se(X) electrostatic contacts. Specifically, the intra-layer tetrahedra separation is governed by the dual Tl(1)---Se(1) interactions formed by adjacent opposite facing tetrahedra. Because the P—Se(1) bond is essentially parallel to the *a* axis, lengthening of this bond causes an expansion of the *a* axis. Although the P—Se(2) bond (which is roughly parallel to the *c* axis) also lengthens, only one Tl(1)---Se(2) interaction is present; the Tl(2)---Se(2) distance is beyond the sum of their ionic radii. Consequently, lengthening of the P—Se(2) bond does not prevent contraction along the *c* axis.

As with the room-temperature structure, Se(X)—P—Se(X) angles are significantly different from the idealized tetrahedral value, with Se(1)-related angles (only) being smaller. Anisotropy of the Tl(2) thermal parameter u_{22} is large; the relative magnitude is comparable to the anisotropy observed for the same parameter at room temperature, which suggests that compression along the *b* axis does little to perturb the Tl(2) freedom of motion in that direction.

Although structural changes do occur in these materials as temperature is reduced, no phase transitions were discovered in either compound, down to 65 K. This is consistent with previous ultrasonic measurements on Tl_3PSe_4, which showed only a gradual softening of the shear wave velocity as a function of temperature (down to 90 K). As a result of high-pressure and ultrasonic measurements on Tl_3PSe_4, Fritz and co-workers (FIGM, 1978) suggested that the soft mode had a much greater intrinsic dependence on volume than temperature and that no temperature-induced phase transition should occur.

If, in fact, a significant reduction in crystal volume is necessary for a phase transition to occur, then volume contractions due to reduced temperature must approach those reached under pressure. Recent high-pressure single-crystal neutron diffraction measurements of Tl_3PSe_4 lattice parameters near the 1.4 GPa transition (Alkire, Larson, Vergamini, Schirber & Morosin, 1985) yielded $a = 9.130$ (4), $b = 10.787$ (4), $c = 8.895$ (3) Å, *i.e.* a 5.5% volume decrease over the room-temperature ambient-pressure structure without

* Lists of structure factors have been deposited with the British Library Lending Division as Supplementary Publication No. SUP 42307 (29 pp.). Copies may be obtained through The Executive Secretary, International Union of Crystallography, 5 Abbey Square, Chester CH1 2HU, England.

Table 1. *Positional and thermal parameters* (Å²) *at* 65 K

Thermal motion of the atoms is defined as $\exp[-2\pi^2(h^2a^{*2}u_{11} + k^2b^{*2}u_{22} + l^2c^{*2}u_{33} + 2hka^*b^*u_{12} + 2hla^*c^*u_{13} + 2klb^*c^*u_{33})]$.

	x	y	z	u_{11}	u_{22}	u_{33}	u_{12}	u_{13}	u_{23}
Tl_3PSe_4									
Tl(1)	0·3058 (1)	0·4522 (1)	0·5584 (1)	0·00792 (18)	0·00649 (17)	0·00825 (16)	−0·00037 (17)	0·00041 (16)	0·00041 (18)
Tl(2)	0·6143 (1)	¼	−0·1114 (1)	0·00717 (28)	0·01787 (36)	0·00593 (24)	0	0·00054 (23)	0
P	0·4717 (1)	¼	0·2819 (1)	0·00396 (40)	0·00488 (42)	0·00426 (35)	0	0·00065 (35)	0
Se(1)	0·2327 (1)	¼	0·3048 (1)	0·00442 (28)	0·00717 (28)	0·00535 (23)	0	−0·00001 (22)	0
Se(2)	0·5659 (1)	¼	0·5069 (1)	0·00492 (27)	0·00793 (30)	0·00391 (23)	0	0·00041 (22)	0
Se(3)	0·5353 (1)	0·0849 (1)	0·1587 (1)	0·00771 (21)	0·00713 (20)	0·00611 (17)	0·00196 (18)	0·00027 (17)	−0·00137 (18)
Tl_3AsS_4									
Tl(1)	0·3046 (1)	0·4512 (1)	0·5631 (1)	0·00913 (13)	0·00648 (13)	0·00934 (18)	−0·00067 (14)	−0·00017 (14)	0·00047 (17)
Tl(2)	0·6097 (1)	¼	−0·1129 (1)	0·00763 (19)	0·01827 (31)	0·00702 (26)	0	0·00023 (20)	0
As	0·4732 (1)	¼	0·2809 (1)	0·00337 (23)	0·00467 (28)	0·00301 (30)	0	−0·00021 (23)	0
S(1)	0·2332 (2)	¼	0·3063 (2)	0·00372 (54)	0·00646 (64)	0·00693 (76)	0	−0·00038 (54)	0
S(2)	0·5681 (2)	¼	0·5053 (2)	0·00532 (53)	0·00842 (71)	0·00489 (75)	0	−0·00047 (56)	0
S(3)	0·5357 (1)	0·0856 (1)	0·1558 (2)	0·00885 (42)	0·00720 (49)	0·00826 (59)	0·00227 (42)	0·00047 (44)	−0·00192 (50)

Table 2. *Distances* (Å) *and angles* (°) *at* 65 *and* 293 K

	Tl_3PSe_4		Tl_3AsS_4	
	65 K	293 K	65 K	293 K
P(As)–X(1)*	2·231 (2)	2·220 (2)	2·193 (2)	2·183 (5)
P(As)–X(2)	2·215 (1)	2·207 (2)	2·169 (2)	2·153 (5)
P(As)–X(3)	2·209 (1)	2·196 (2)	2·169 (2)	2·166 (4)
X(1)–P(As)–X(2)	107·92 (5)	107·92 (10)	107·55 (8)	107·61 (19)
X(1)–P(As)–X(3)	108·25 (4)	108·29 (6)	108·21 (5)	108·06 (12)
X(2)–P(As)–X(3)	110·96 (4)	110·83 (6)	111·43 (5)	111·16 (12)
X(3)–P(As)–X(3′)	110·39 (5)	110·57 (9)	109·88 (8)	110·64 (16)
Tl(1)–X(1)	3·265 (1)	3·262 (2)	3·214 (2)	3·217 (4)
Tl(1)–X(1)	3·168 (1)	3·181 (2)	3·080 (2)	3·091 (4)
Tl(1)–X(2)	3·316 (1)	3·324 (1)	3·274 (1)	3·285 (4)
Tl(1)–X(3)	3·294 (1)	3·313 (2)	3·229 (2)	3·250 (4)
Tl(1)–X(3)	3·322 (1)	3·331 (1)	3·225 (2)	3·228 (4)
Tl(2)–X(1)	3·312 (1)	3·316 (2)	3·198 (2)	3·207 (5)
Tl(2)–X(2)	3·159 (1)	3·155 (2)	3·110 (2)	3·110 (5)
Tl(2)–X(3)	3·129 (1)	3·150 (2)	3·047 (2)	3·077 (4)
X(3)–Tl(2)–X(3)	70·88 (3)	69·90 (4)	71·29 (6)	70·74 (8)

* X = Se,S.

Table 3. *Distances corrected for riding motion and non-correlated motion* (*Busing & Levy*, 1964)

	Tl_3PSe_4		Tl_3AsS_4	
	65 K	293 K	65 K	293 K
P(As)–X(1)*	2·232	2·224	2·194	2·188
P(As)–X(2)	2·215	2·210	2·170	2·156
P(As)–X(3)	2·211	2·206	2·172	2·177
Tl(1)–X(1)	3·261	3·246	3·210	3·202
Tl(1)–X(1)	3·164	3·164	3·076	3·075
Tl(1)–X(2)	3·313	3·308	3·269	3·270
Tl(1)–X(3)	3·318	3·315	3·220	3·212
Tl(1)–X(3)	3·289	3·292	3·223	3·230
Tl(2)–X(1)	3·306	3·294	3·192	3·186
Tl(2)–X(2)	3·152	3·133	3·104	3·089
Tl(2)–X(3)	3·124	3·133	3·042	3·059

* X = Se,S.

any noticeable phase change. Given that the volume change in Tl_3PSe_4 is only 0·5% on going from 293 to 65 K, no phase change is to be expected upon further reduction in temperature. For Tl_3AsS_4, two pressure-induced structural phase transitions have been determined, the first occurring at 2·1 GPa, but no comparable temperature-dependent ultrasonic data are available. However, given the structural similarities between these materials and that the first pressure-related phase change in Tl_3AsS_4 requires a 0·7 GPa increase relative to Tl_3PSe_4 (even though the soft mode in Tl_3AsS_4 does not reach zero velocity at this point), it is unlikely that a temperature-related phase change could be induced upon further reduction in temperature.

The present work represents a twofold increase in precision over the previous neutron structure determination with only small changes occurring in atom positions. Thermal motion of atom Tl(2) is highly anisotropic and similar to that observed at room temperature, despite a significant decrease in the *b* lattice parameter. In accordance with results obtained by Fritz and co-workers (FIGM, 1978) no phase transitions were observed for these compounds at 65 K. In addition, lattice parameters determined from this study and a recent high-pressure neutron diffraction study show that it is highly unlikely for any temperature-induced phase transition to occur in these materials, given the strong volume dependence for such transitions as determined by Fritz and co-workers (FIGM, 1978).

The authors gratefully thank A. C. Lawson for his valuable assistance in performing temperature calibrations and Milton Gottlieb of Westinghouse Research for supplying the crystals used in this experiment. This work was performed under the auspices of the US Department of Energy, supported in part by Contract W-7405-ENG-36 and Contract DE-AC-0476-Dp00789.

References

ALKIRE, R. W., LARSON, A. C., VERGAMINI, P. J., SCHIRBER, J. E. & MOROSIN, B. (1985). *J. Appl. Cryst.* **18**, 145–149.

ALKIRE, R. W., VERGAMINI, P. J., LARSON, A. C. & MOROSIN, B. (1984). *Acta Cryst.* C**40**, 1502–1506.

BORKOWSKI, C. J. & KOPP, M. K. (1978). *J. Appl. Cryst.* **11**, 430–434.

BUSING, W. R. & LEVY, H. A. (1964). *Acta Cryst.* **17**, 142–146.
FRITZ, I. J., GOTTLIEB, M., ISAACS, T. J. & MOROSIN, B. (1981). *J. Phys. Chem. Solids*, **42**, 269–273.
FRITZ, I. J., ISAACS, T. J., GOTTLIEB, M. & MOROSIN, B. (1978). *Solid State Commun.* **27**, 535–539.
GARBER, D. I. & KINSEY, R. R. (1976). *Neutron Cross Sections.* BNL 325, 3rd ed., Vol. III. Brookhaven National Laboratory, Upton, NY.
GOTTLIEB, M., ISAACS, T. J., FEICHTNER, J. D. & ROLAND, G. W. (1974). *J. Appl. Phys.* **45**, 5145–5151.
JOHNSON, C. K. (1976). *ORTEP*II. Report ORNL-5138. Oak Ridge National Laboratory, Tennessee.
KOESTER, L. & YELON, W. B. (1982). *Compilation of Low Energy Neutron Scattering Lengths and Cross Sections.* ECN, Netherlands Energy Research Foundation, Department of Physics.
LARSON, A. C. (1977). *Program and Abstracts.* American Crystallographic Association Summer Meeting, East Lansing, Michigan, paper H8, p. 67.
MUGHABGHAB, S. F. & GARBER, D. I. (1973). *Neutron Cross Sections.* BNL 325, 3rd ed., Vol. I. Brookhaven National Laboratory, Upton, NY.
SCHULTZ, A. J. (1984). Private communication.
VERGAMINI, P. J., LARSON, A. C. & ALKIRE, R. W. (1985). In preparation.

Acta Cryst. (1985). C**41**, 1714–1717

Ammonium Trifluoroberyllate. High-Temperature Phases I and II

BY A. WAŚKOWSKA

Institute of Low Temperature and Structure Research, Polish Academy of Sciences, 50–950 Wrocław, Pl. Katedralny 1, Poland

(*Received* 15 *February* 1985; *accepted* 12 *August* 1985)

Abstract. $[NH_4][BeF_3]$, $M_r = 84{\cdot}05$; phase I: orthorhombic, *Pmnb*, $a = 5{\cdot}743\ (5)$, $b = 4{\cdot}643\ (5)$, $c = 12{\cdot}789\ (2)$ Å, $V = 341{\cdot}0\ (2)$ Å^3, $Z = 4$, $D_m = 1{\cdot}63\ (2)$, $D_x = 1{\cdot}637\ (3)$ Mg m^{-3}, λ(Mo $K\alpha$) $= 0{\cdot}7107$ Å, $\mu = 0{\cdot}94$ mm^{-1}, $F(000) = 168$, $T = 386$ K, final $R = 0{\cdot}057$ for 287 observed reflections; phase II: orthorhombic, $P2_12_12_1$, $a = 5{\cdot}661\ (4)$, $b = 4{\cdot}600\ (5)$, $c = 12{\cdot}990\ (3)$ Å, $V = 338{\cdot}3\ (4)$ Å^3, $Z = 4$, $D_x = 1{\cdot}650\ (3)$ Mg m^{-3}, λ(Cu $K\alpha$) $= 1{\cdot}5418$ Å, $\mu = 2{\cdot}04$ mm^{-1}, $T = 295$ K, final $R = 0{\cdot}051$ for 419 observed reflections. Phase II is metastable at room temperature which allowed data collection at room temperature. Both high-temperature phases are closely related to the ferroelastic phase III [Waśkowska (1983). *Acta Cryst.* C**39**, 1167–1169]. Rigid BeF_4 groups preserve nearly the same shape through the phase transition. Temperature-induced motion of the rigid molecular units leads to pronounced changes in conformation of the $(BeF_4)_n$ chains and through a system of hydrogen bonds of N—H···F type causes reorientation of NH_4^+ ions during phase transition.

Introduction. NH_4BeF_3 belongs to the family of ferroelastic hydrogen-bonded crystals and on heating undergoes phase transitions at $T_3 = 252{\cdot}2$, $T_2 = 334{\cdot}3$ and $T_1 = 347{\cdot}3$ K. At room temperature the crystal is ferroelastic (Makita & Suzuki, 1980; Czapla, Czupiński & Waśkowska, 1982). Thermogravimetric analysis, measurements of specific heat (DSC), X-ray studies of lattice parameters as a function of temperature, and Weissenberg photographs performed in temperature regions corresponding to particular phases led to the following phase diagram (Łukaszewicz, Waśkowska, Tomaszewski & Czapla, 1983):

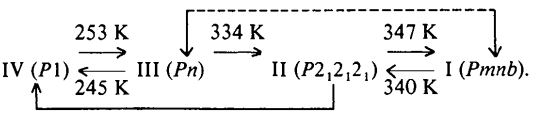

The crystals were grown from an aqueous solution of phase III. On heating, they transform at T_2 to the intermediate phase II. On cooling, the sequence of the phases is I → II → IV, *i.e.* phase II transforms directly to phase IV. Below room temperature both phases II and III transform at $T_3' = 245$ K to phase IV, which on heating returns to the room-temperature phase III. The X-ray crystal structure of the room-temperature phase was described by Waśkowska (1983). In the present paper the structures of the high-temperature phase I and of the intermediate phase II are determined and compared with the phase III in an attempt to find a molecular phase-transition mechanism in NH_4BeF_3.

Experimental. *Phase* I. Growth conditions described by Czapla *et al.* (1982). D_m by flotation in dibromoethane/chloroform. Cylinder-shaped sample from the plate elongated in **b** ($r = 0{\cdot}15$, $l = 0{\cdot}37$ mm) heated to 358 (2) K. Lattice parameters from eight high-angle reflections in range $63{\cdot}3 \le \theta \le 82{\cdot}5°$ measured as function of temperature on a Bond diffractometer using Cu $K\alpha$ radiation (Łukaszewicz *et al.*, 1983). Stoe STADI-2 two-circle diffractometer (Mo $K\alpha$ radiation,

0108-2701/85/121714-04$01.50